

NATIONAL RADIO ASTRONOMY OBSERVATORY
Charlottesville, VA

ELECTRONICS DIVISION TECHNICAL NOTE NO. 224

S-Parameter Measurements of an SAO Edge-Mode Isolator at 4 K

Philip Dindo

October 31, 2019

S-Parameter Measurements of an SAO Edge-Mode Isolator at 4 K

Philip Dindo and A.R. Kerr

31 October 2019

Introduction

In a radio receiver the mixer generally has an output impedance that is different from the input impedance of the IF amplifier. Some mixers may also exhibit negative output resistance. To reduce the interaction between mixer and amplifier a ferrite isolator is often used. However, the insertion loss of the isolator can contribute substantially to the overall system noise temperature.

Until recently, the only cryogenic low loss isolators for the 4-20 GHz range were of the Y-junction type, and the bandwidth of these was limited to about an octave, or 3:1 with increased loss. Now a field displacement isolator, also called an edge-mode isolator, has been optimized for cryogenic operation with low loss over much wider bandwidths.

Marion Hines was the first to use the propagation characteristics of striplines on ferrites to prototype a wideband field-displacement isolator [1]. Subsequently, the Smithsonian Astrophysical Observatory (SAO) group reported a 5 to 18 GHz isolator with 2 dB insertion loss in 2015 [2]. In 2018, the same group reported a multi-octave 4-20 GHz isolator [3] with even better characteristics and specifically made to meet the requirements of the wideband sub-millimeter array (wSMA) [4].

We obtained an isolator from SAO for cryogenic testing at the National Radio Astronomy Observatory (NRAO), to evaluate it as a candidate for an upgraded ALMA Band6 Version 2 receiver for which the IF band will probably be 4-16 GHz.

SAO Isolator Design

The edge-mode isolator shown in Figure 1 [3] has dimensions of 40 x 33 x 15 mm (excluding the 2.92 mm connectors). It was optimized for use between the SIS mixer and IF amplifier on the wSMA receivers which have a 4 to 20 GHz IF. The design specifications are divided into two frequency ranges as shown in Figure 1. Between 4 and 12 GHz, the insertion loss is not to exceed 0.7 dB and the isolation should exceed 15 dB. Between 12 and 20 GHz, these parameters are somewhat relaxed to allow for practical implementation of this isolator. Over the entire frequency range the return loss must exceed 15 dB.

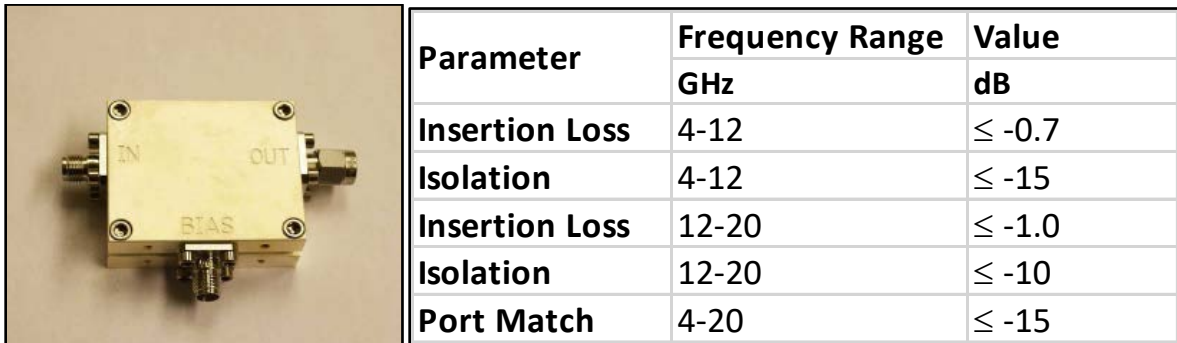


Fig. 1. Photograph of the SAO isolator and the design specifications. Dimensions without the connectors: 40x33x15 mm. From [3].

The disassembled isolator is shown in Figure 2. A copper 50-Ohm stripline is sandwiched between two ferrite substrates which have a relative dielectric constant of about 14.1. The stripline circuit near the bias port is sandwiched between two absorber plates. A neodymium block magnet produces a bias field perpendicular to the ferrite surface. The DC bias port is for biasing a mixer connected to the input of the isolator, but the termination of this port does not substantially affect the isolator's microwave performance.

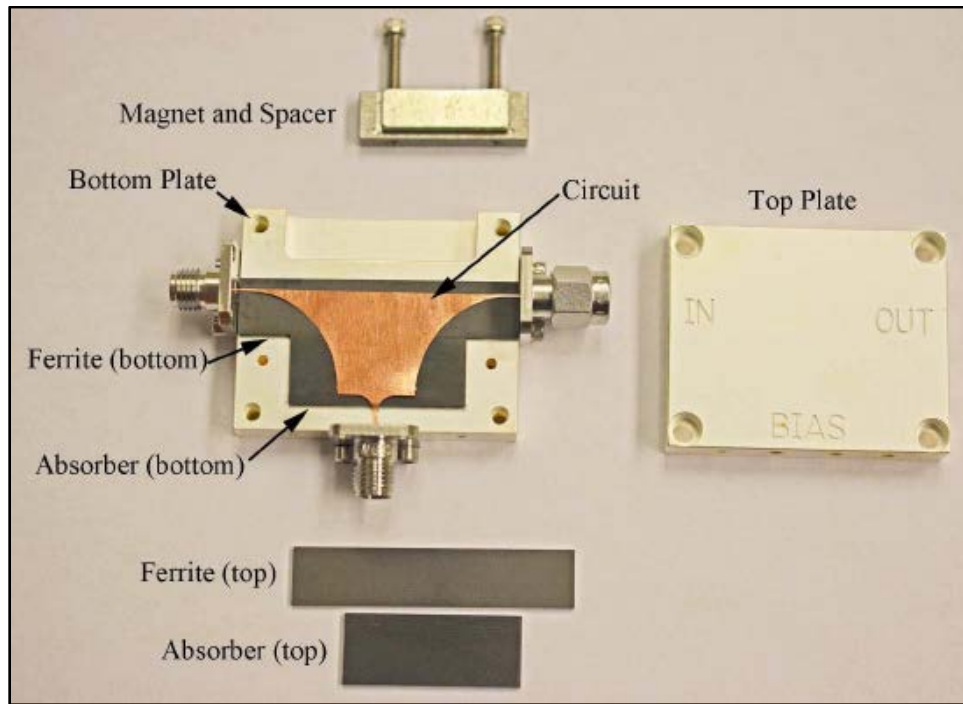


Fig. 2. Photograph of the disassembled SAO isolator showing a split-block assembly with the tapered stripline sandwiched between a ferrite substrate and an absorber. From [3].

Cryogenic Setup for S-Parameter Measurements

Figure 3 shows the cryostat used for measurement of microwave devices at 4 K. The microwave S-Parameter measurement is conducted by Keysight PNA-X Model N2545A with Automatic Fixture Removal Software [5].

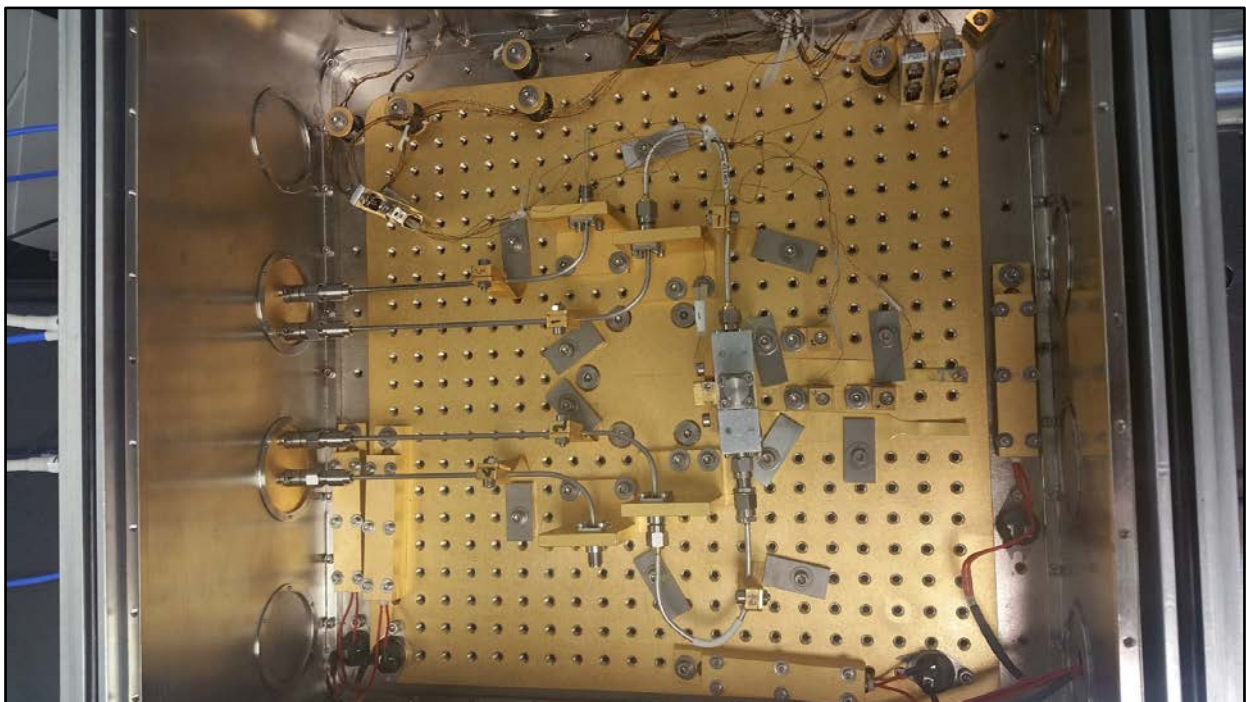


Fig. 3. Photograph of the cryostat used for microwave measurements at 4 K. The SAO isolator is shown connected on each side to a 180° bent silver plated copper coaxial cable, then to a 90° bent stainless steel coaxial cable, and to a coaxial adapter attached to a round-shaped test-pod on the wall of the cryostat (barely visible at the top right corner). A silicon-diode temperature sensor is connected to the isolator. The test-pod chamber housing contains a coiled stainless-steel coaxial cable and serves to isolate the cold temperature inside the cryostat from the outside. Coaxial cables from the PNA-X are connected to the test-pod via coaxial adapters.

In cryogenic VNA measurements one of the difficult measurement tasks is to de-embed the effects of the multiple coaxial cables and adapters leading from the calibration planes of the VNA to the device under test. Each channel consists of the following cables and adapters:

- At room temperature: female to male K-connector adaptor (Fairview, Part # SM-3240)
- At room temperature: female to female K-connector Vacuum feedthrough (Fairview, Part # SM-3224)
- Room temperature to 77 K: stainless steel looped coaxial cable with male and female K-connector ends (UT-85-SS-SS, length = 6.198” or 157.4 mm)
- 77 K to 4 K: stainless steel coaxial cable with male and female K-connector ends (UT-85-SS-SS, length = 7.26” or 184.4 mm)
- 4 K heatsink to DUT: copper/silver plated copper-weld coaxial cable with two male K-connector ends (UT-85 –TP Copper/SPCW center conductor, length = 5.3” or 134.6mm).

Figure 4 shows schematically the use of Keysight’s Automatic Fixture Removal (AFR) software. The cable chains leading to the ports of the device under test are designated as 2-port fixtures S_A and S_B . AFR software uses time domain measurements with short-circuit calibration standards to identify the discontinuities and location of the desired reference planes. Frequency domain data taken with both short and through calibration standards are then used to compute the S-parameters of fixtures S_A and S_B .

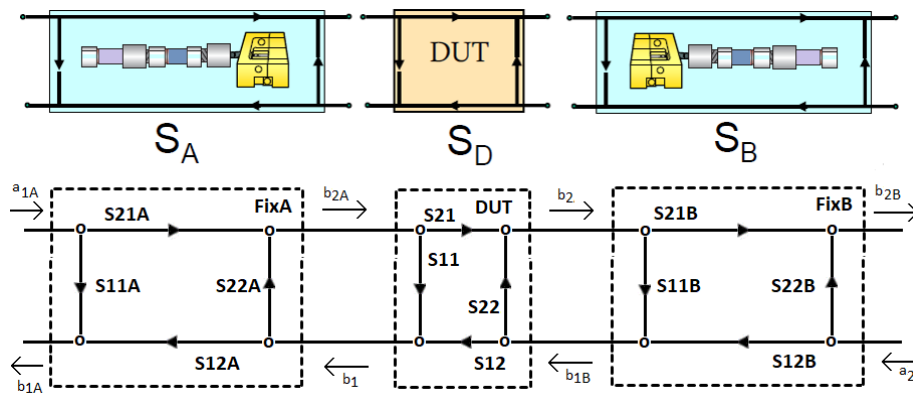


Fig. 4. Keysight’s Automatic Fixture Removal software computes the fixture S-Parameters and then de-embeds the coaxial cables and adapters leading to the device under test.

S-Parameter Measurement Errors Due to AFR

One of the questions regarding measurements with Keysight’s AFR module concerns the accuracy of the resulting S-parameters. A conclusive answer would be obtained by measuring the S-parameters of the device inside the cryostat, and compare them with those measured directly on the PNA-X. While this is not possible at 4 K, it is possible at room temperature. While the measurement errors at room temperature may not be fully indicative of the errors at 4 K, the information obtained by room temperature measurement comparison is informative and sheds light on the magnitude of the errors.

Figure 5 shows the insertion loss of the SAO isolator measured directly at the PNA-X calibration ports (solid blue), and measured inside the cryostat using AFR (dotted blue). Both measurements were conducted at room temperature. The dB difference between the two measurements is the error (red trace).

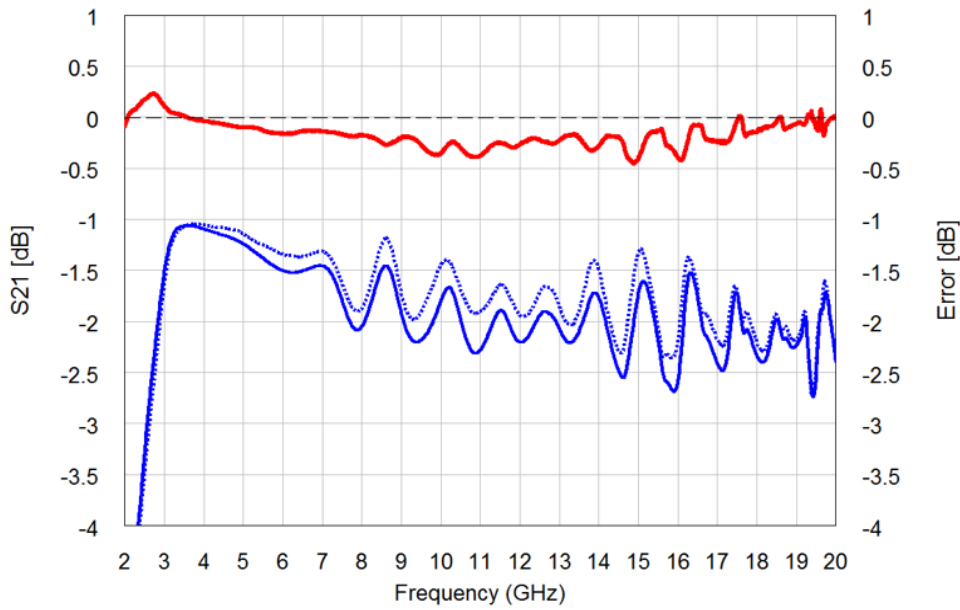


Fig. 5. Inset loss S21 of SAO isolator at room temperature.

- Solid blue trace: S21, direct insertion loss measurement at the VNA calibration planes -- (left scale).
- Dotted blue trace: AFR S21, insertion loss measurement in the cryostat -- (left scale).
- Red trace: the error difference in dB between the two S21 measurements -- (right scale).

The insertion loss at room temperature (which is generally greater than at 4 K) varies between 1 and 3 dB. The frequency band also is shifted at cold temperatures. Figure 5 shows that the error in the insertion loss measurement using AFR in the 4-20 GHz frequency range is less than 1/2 dB peak-to-peak. Note that the error is highest at the peaks of the response ripples.

The isolation, S12, at room temperature shown in Figure 6 indicates that measurements direct to calibration plane and de-embedded using AFR are very close. The error from using AFR is less than 1/2 dB. Also, note that the error is highest at the peaks of the response ripples.

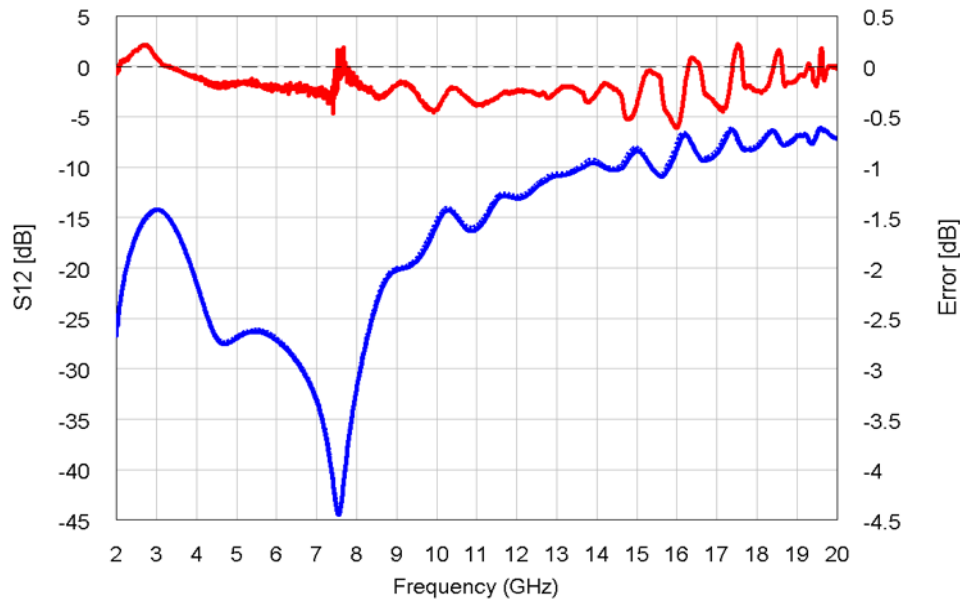


Fig. 6. Isolation S12 of SAO Isolator at Room Temperature.

- Solid blue trace: S12, direct isolation measurement at the VNA calibration planes -- (left scale).
- Dotted blue trace: AFR S12, isolation measurement in the cryostat -- (left scale).
- Red trace: the error difference in dB between the two S12 measurements -- (right scale).

The error in return loss due to AFR de-embedding is shown in Figure 7. The direct and de-embedded measurements are quite similar, but the errors are again greatest at the peaks of the response ripples.

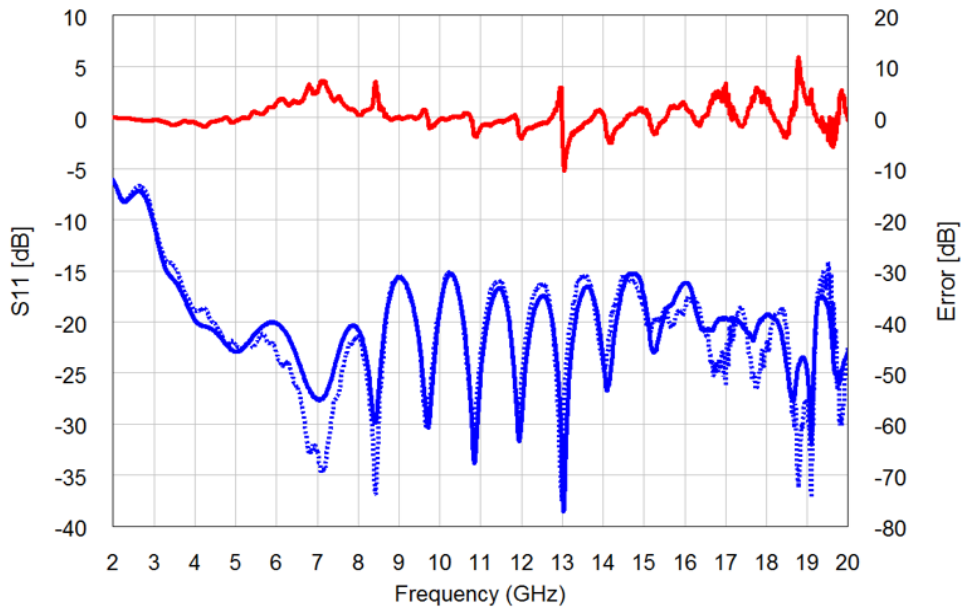


Fig. 7. Input Return Loss S11 of SAO Isolator at Room Temperature.

- Solid blue trace: S11, direct input return loss measurement at the VNA calibration planes -- (left scale).
- Dotted blue trace: AFR S11, input return loss measurement in the cryostat -- (left scale).
- Red trace: the error difference in dB between the two S11 measurements – (right scale).

S-Parameter Measurement of SAO Isolator at 4K

The 2-20 GHz S-Parameters measured at 4 K using AFR are shown in Figure 8. Within the uncertainty of the measurements, all parameters are consistent with the specifications in Figure 1.

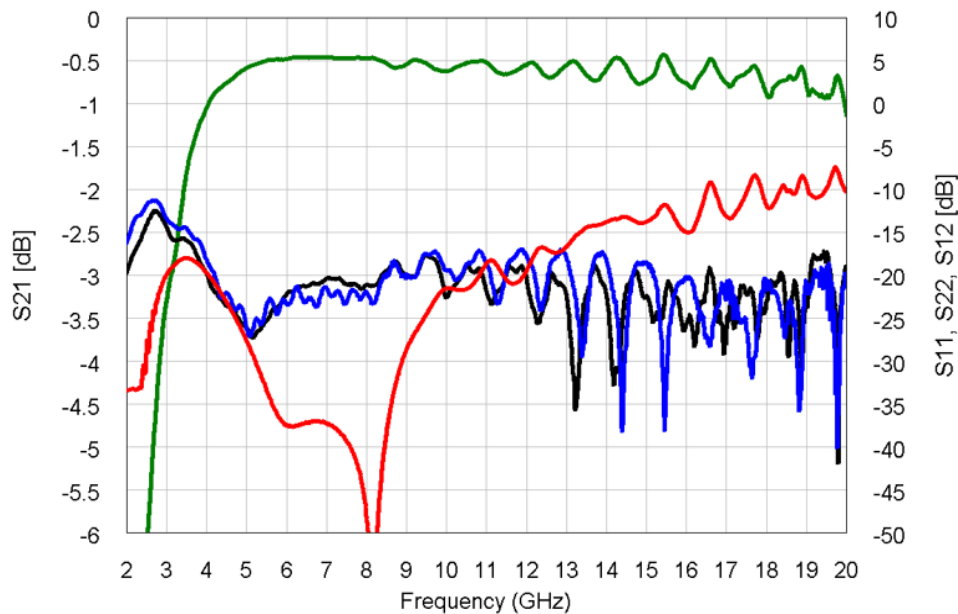


Fig. 8. Measured S-parameters of the SAO isolator at 4 K.

- Green trace: S21, insertion loss -- (left scale).
- Red trace: S12, isolation – (right scale).
- Blue trace: S11, input return loss – (right scale).
- Black trace: S22, output return loss – (right scale).

The insertion loss is ~1 dB at 4 GHz but improves to ~0.5 dB from 5 to 8 GHz, then increases gradually to ~1 dB at 20 GHz. Above 4 GHz, the input and output return losses are ~20 dB, while the isolation is >15 dB from 4 to 13 GHz, decreasing to ~10 dB at 20 GHz.

Acknowledgments

The author thanks Edward Tong of SAO for the loan of the isolator evaluated in this report.

References

- [1] M. E. Hines, "Reciprocal and nonreciprocal modes of propagation in ferrite stripline and microstrip devices," IEEE Trans. Microwave Theory and Techniques, vol. MTT-19, no. 5, pp. 442–451, May 1971.
- [2] L. Zeng, C.-Y. E. Tong, R. Blundell, and R. S. Kimberk, "A wideband edge-mode isolator for cryogenic operation," in Proc. 26th Int. Symp. Space THz Technol., 2015, p. 45.
- [3] L. Zeng, C.-Y. E. Tong, R. Blundell, R. Grimes, and S. Paine, "A Low-Loss Edge-Mode Isolator With Improved Bandwidth for Cryogenic Operation," in IEEE Trans. Microwave Theory and Techniques, vol. MTT-66, no. 5, pp. 2154–2160, May 2018.
- [4] P. Grimes, R. Blundell, S. Paine, C.-Y. E. Tong, and L. Zeng, "Next generation receivers for the submillimeter array," Proc. SPIE, vol. 9914, p. 991424, Jul. 2016.
- [5] Keysight Technologies, Automatic Fixture Removal Software, www.keysight.com

Revision Notes

Original EDTN 224, 31 October 2019.